Biosensors and Bioelectronics 203 (2022) 114023

Contents lists available at ScienceDirect

Biosensors and Bioelectronics

journal homepage: www.elsevier.com/locate/bios

Ultrasensitive detection of small biomolecules using aptamer-based molecular recognition and nanoparticle counting

Ruiting Xu [a,1], Lidya Abune [b,1], Brandon Davis [b], Leixin Ouyang [a], Ge Zhang [c], Yong Wang [b,*], Jiang Zhe [a,**]

[a] Department of Mechanical Engineering, University of Akron, Akron, OH, 44325, United States
[b] Department of Biomedical Engineering, Pennsylvania State University, State College, PA, 16801, United States
[c] Department of Biomedical Engineering, University of Akron, Akron, OH, 44325, United States

ARTICLE INFO

Keywords:
Biomolecule detection
Aptamer
Nanoparticles
Adenosine
Resistive pulse sensor

ABSTRACT

Detection of small biomolecules is critical for understanding molecular mechanisms in biological systems and performing in vitro diagnosis in clinics. Current antibody based detection methods face large challenges in detecting small biomolecules at low concentrations. We report a new method for detecting small biomolecules based on molecular recognition and nanoparticle (NP) counting. Aptamer-functionalized NPs are attached to complementary sequence (CS)-conjugated microparticle (MP) carriers. In the presence of target small biomolecules at ultra low concentrations, NPs would be released from the MP carriers. Coupled with a resistive pulse sensor (RPS) using a micropore that counts the released NPs, this method can measure the concentrations of target biomolecules at low concentrations with high sensitivity and high throughput. Adenosine was used as a model to demonstrate the feasibility of this method. It is demonstrated that this method can detect a wide range of adenosine concentrations with a low detection limit of 0.168 nM, which is 10 times lower than that of the ELISA kit. With its simple structure, high sensitivity, and high reproducibility, this detection method holds great potential for the ultrasensitive detection of low abundance small biomolecules.

1. Introduction

A variety of small biomolecules (e.g., adenosine) play important roles in regulating the metabolism of cells and living organisms (Wang et al., 2018). In addition, many small biomolecules (e.g., drugs) are highly potent even at an ultra low concentration. An ability to detect them is critical for understanding molecular mechanisms in biological systems and performing in vitro diagnosis to monitor the progression of health problems. Thus, great efforts have been made to develop ultrasensitive methods for the detection of small biomolecules (Liu and Lu, 2005, 2006a, b; Sexton et al., 2007; Wang et al., 2006; Wang et al., 2018). However, while elegant methods such as polymerase chain reaction (PCR) (Garibyan and Avashia, 2013; Green et al., 2015; Powledge, 2004) and enzyme-linked immunosorbent assay (ELISA) (Chen et al., 2018; Wright et al., 1993) have been well-established for the ultrasensitive detection of large biomolecules such as nucleic acids and proteins, it is not simple to tune these methods for the detection of small biomolecules. For instance, ELISA may not be applicable to small biomolecules that have an ultra-low surface area and cannot easily accommodate a pair of antibodies (Sakamoto et al., 2018). Thus, there remains a great need to explore new methods for the ultrasensitive detection of small biomolecules.

Aptamers, short single-stranded oligonucleotides, are an emerging class of affinity ligands. They have high specificity and sensitivity against target analytes. They can be chemically synthesized and modified with high stability in harsh working environment. They can also undergo conformational changes in response to analytes or their complementary sequences (Kalra et al., 2018; Ni et al., 2021; Ruscito and DeRosa, 2016; Song et al., 2008). Thus, aptamers have been applied to functionalize nanomaterials in developing biosensors or bioelectronics for molecular sensing. For example, a classic biosensing mechanism has been developed by coupling aptamer-functionalized gold NP and optical detector (Fu et al., 2020). The purple aggregates formed by aptamer-functionalized gold NPs would turn into red dissociated NPs in

* Corresponding author.
** Corresponding author.
E-mail addresses: yxw30@psu.edu (Y. Wang), jzhe@uakron.edu (J. Zhe).
[1] R.X. and L.A. contributed equally.

https://doi.org/10.1016/j.bios.2022.114023
Received 20 October 2021; Received in revised form 11 January 2022; Accepted 17 January 2022
Available online 23 January 2022

the presence of analytes. Similarly, separate NPs can be induced to form aggregates, which induces the change of the color from red to purple. This color transformation could be used as a detectable optical signal. Inspired by these elegant works, other NP-based sensors have also been developed (Chang et al., 2019; Liu et al., 2018b; Maysinger et al., 2015). Despite these advances, the development of aptamer-based sensors with low detection limit and broad detection range is still challenging.

Resistive pulse sensor (RPS) based on Coulter counting principle have demonstrated great advantages when used to detect micro and nanoscale bio-objects. With a simple structure, RPS can rapidly detect targeted analytes and perform individual measure (e.g. size, surface charge, mobility) with high resolution. It has been used for detecting different types of biomolecules such as proteins (Sexton et al., 2007; Sha et al., 2013), peptides (Heaton and Platt, 2019; Maugi et al., 2020), and DNAs (Arima et al., 2018; Harrell et al., 2006; Yang and Yamamoto, 2016; Zhou et al., 2011). Previously, we have explored to integrate microfluidic RPS with various novel bioassays to further improve the detection capabilities of RPS. (Han et al., 2014, 2016; Liu et al., 2018a). Our promising results strongly suggest the great potential of using RPS for ultrasensitive biomolecule detection. However, antibody based biomolecule detection methods have difficulty in detecting small molecules at low concentrations (Liu and Lei, 2021; Prante et al., 2020; Wang et al., 2018); their stability and reproducibility are affected by environment (e.g. temperature fluctuations, variations in pH) (Byrne et al., 2009; Hahm and Bhunia, 2006; Hearty et al., 2006). Further, while nanopore based RPS was commonly chosen to detect biomolecules (Tang et al., 2020; Yang and Yamamoto, 2016) the detection is limited by the low throughput and potential blockage.

To overcome the above limitations, we integrated aptamer modified NPs based small biomolecule detection and high throughput NP counting system via a micropore based RPS into one biosensing system. The purpose of this work was to study the feasibility of integrating analyte-induced aptamer reconfiguration and microfluidic RPS into one biosensing system for the detection of small molecules. Adenosine and its aptamer were used as a model. Silica NPs (SNPs) were functionalized with adenosine aptamer. A microparticle (MP) carrier was functionalized with the complementary sequence (CS) of the aptamer for displaying the NPs. NPs were counted using a customized micropore-based resistance pulse sensor. The concentration of adenosine was varied from 0.1 nM to 10 mM to illustrate the sensitivity and range of detection.

2. Material and methods

2.1. Principle

Fig. 1a illustrates the new biomolecule detection principle. This method consists of two major components: 1) a target-responsive aptamer-based SNP release system and 2) a microfluidic RPS for counting SNPs. In the first component, aptamer-modified SNPs are attached to CS-conjugated MPs via hybridization. In the presence of the aptamer's target molecule, the aptamers will undergo a conformational shift and SNPs will be detached from the CS-conjugated MPs. The

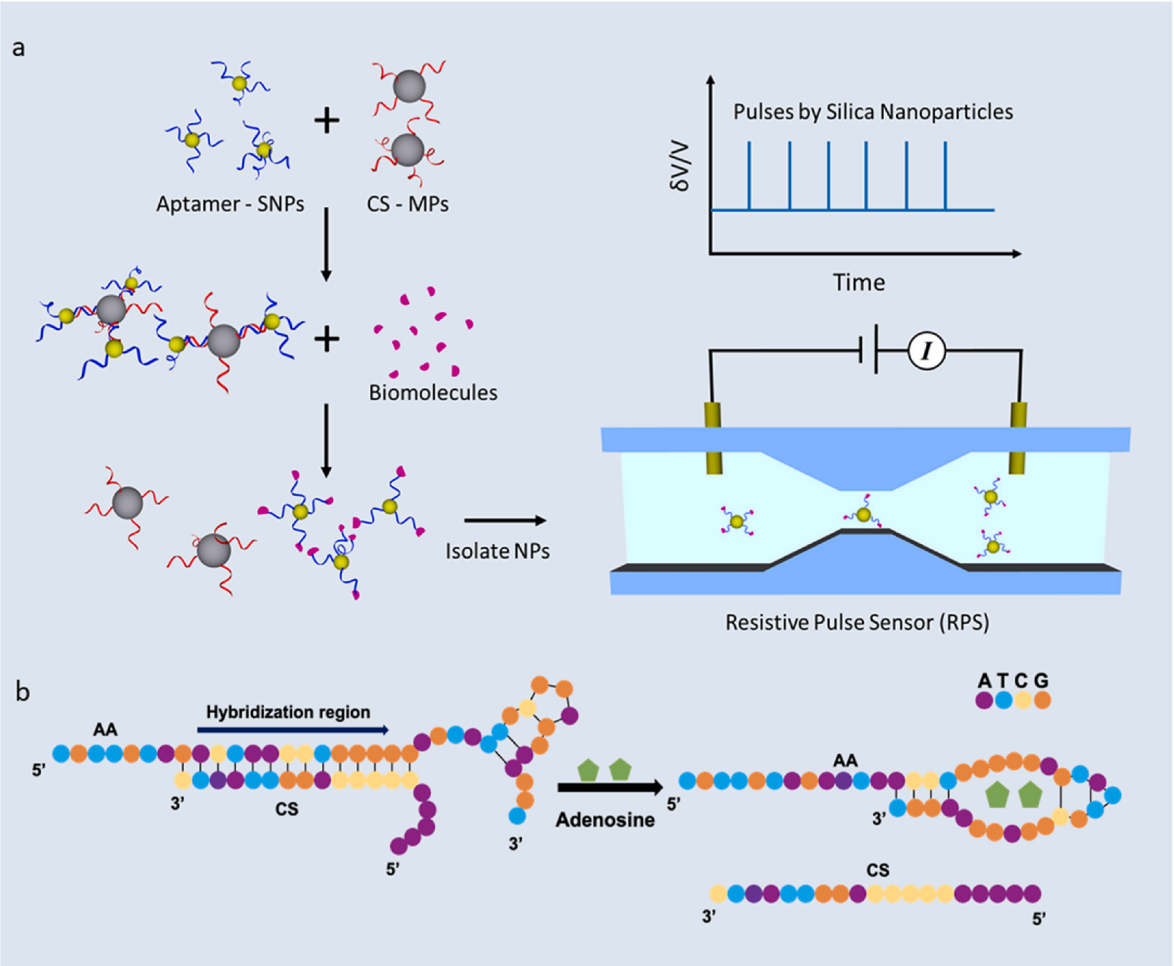

Fig. 1. Mechanism of detecting small biomolecules via aptamer reconfiguration and NP counting. (a): Target biomolecules induce the release of NPs from MPs. The released NPs are counted by RPS. (b) Target-induced molecular reconfiguration of aptamer and separation of aptamer-CS duplex (AA: adenosine aptamer, CS: complementary sequence).

adenosine aptamer has been previously identified and well-studied (Huizenga and Szostak, 1995; Lin and Patei, 1997). The aptamer sequence (5′- TGTTGTAGACTAACCTGGGGGAGTATTGCGGAGGA AGGT-3′) used in this study was modified to enhance the reversible SNP-MP interaction. This adenosine aptamer contains three functional regions. The first twenty-seven nucleotides at the 3′ end bind to adenosine; the middle region is complementary to a portion of CS; and a seven nucleotide spacer was added at the 5′ end to avoid potential steric hindrance of molecular interactions. Meanwhile, the CS sequence (5′AAAAACCCCCAGGTTAGTC-3′) was designed to contain fourteen nucleotides that can bind to the aptamer sequence (Table S1). This 14 base-pair hybridization region was selected to ensure the stable formation of the CS-aptamer duplex, while allowing adenosine to induce CS displacement upon binding the aptamer (Lai et al., 2017). Similarly, a five nucleotide space was added at the 5′ end of CS to avoid potential steric hindrance. Each sequence has been modified with a biotin group at the 5′ end. The adenosine aptamer and CS interactions are shown in Fig. 1b.

The second component is a microfluidic RPS with a micropore (including inlet/outlet reservoirs) that measures the released SNPs based on the Coulter counting principle. The amount of released SNPs corresponds to the concentration of biomolecules. Therefore, by simply counting the released SNPs, the concentration of target biomolecules can be determined digitally with high resolution. In our approach, aptamer-conjugated SNPs (~490 nm) were attached onto the surface of CS-modified MPs via intermolecular CS-aptamer hybridization. Note that although smaller sized NPs (e.g., 100 nm) could be used to improve the biomolecule detection sensitivity (Billinge and Platt, 2015), a nanopore would have to be fabricated using expensive nanofabrication facilities. Further, only a very low sample volume would be analyzed with a nanopore.

2.2. Conjugation of DNA sequences to particles

Streptavidin-modified SNPs (~490 nm) and magnetic MPs (~5 μm) were obtained from Spherotech (Lake Forest, IL). The adenosine binding aptamer sequence and CS were selected based on a previously published study (Sexton et al., 2007). These oligonucleotide sequences were custom ordered with a biotin modification at the 5′ end from Integrated DNA technologies (Coralville, IA). For the modification of SNPs, 1 mg of particles were reacted with 3 nmole aptamer in 200 μL binding buffer solution (10 mM Tris, 1 mM EDTA, 2 M NaCl) at 4 °C overnight. Similarly, 10 mg of MPs were reacted overnight with 8 nmole of CS in 200 μL binding buffer solution at 4 °C. After the reaction, the particles were pelleted and washed in Dulbecco's phosphate-buffered saline (DPBS, 1X, product # MT21031CV, Thermo Fisher Scientific) five times to remove the excess DNA. The amount of DNA that remained in the supernatant was measured via Nanodrop 2000. The amount of DNAs which remained in the supernatant were subtracted from the total amount of DNA used for the reaction to estimate the amount of DNA conjugated to the particles (Supplementary Information, Section 2). The conjugation was verified by assessing the zeta potential of the particles before and after DNA modification using a Zetasizer Nano ZS (Malvern Panalytics). Note that, while the concentrations and types of ions in the buffer might influence the performance of the aptamer (Hetzke et al., 2019; Hianik et al., 2007; Mayne et al., 2018), in all our experiments we used the same commercially available DPBS buffers (Dulbecco's formula, Calcium Chloride 0.10 g/L, Potassium Chloride 0.2 g/L, Potassium Dihydrogen Phosphate 0.2 g/L, Magnesium Chloride Hexahydrate 0.1 g/L, Sodium Chloride 8 g/L, Disodium Phosphate Heptahydrate 2.1716 g/L), which are unlikely to have a significant effect on the functions of the aptamers, as proved by our experiments.

2.3. Microfluidic RPS and the measurement circuit

The design of the microfluidic RPS for counting SNPs is illustrated in Fig. 2a. The microfluidic RPS consists of 3 main components: 1) a micro pore/channel, 2) a pair of Ag/AgCl electrodes for counting the released, and 3) inlet/outlet reservoirs. The micropore measures 2 μm × 2 μm x 10 μm (width x height x length), while the reservoirs are 3 mm in diameter. An electric field is applied across the Ag/AgCl electrodes to measure the change in resistance within the channel. When a SNP passes through the micropore, it temporarily distorts the electrical field which results in an increase in the channel's resistance and a voltage pulse (Peng and Li, 2018). The magnitude of the pulse reflects the NP's dimension (DeBlois and Bean, 1970; Song et al., 2017). Fig. 2b shows the measurement circuit, where R_1 and R_2 are fixed value resistors, and their resistance are set to be the same (1 k Ohms) to divide the input voltage from the power supply. R_3 represents the resistance of the channel, and R_4 is an external adjustable resistor used to form a Wheatstone bridge. Before each test, R_4 was adjusted to be equal to R_3, so that the voltage drop between A and B (V_{AB}) is zero. When a released SNP passes through the micropore, a resistive change in R_3 is induced and causes a change in V_{AB}. This voltage change is amplified and measured as V_{out}. Each voltage pulse represents the passage of one SNP. Thus by counting the voltage pulses, the number of released SNPs can be determined.

The RPS was fabricated by using standard soft lithography method. An SU8 mold was fabricated using photolithography that is complementary to the following components: (1) a 2 μm × 2 μm x 10 μm (width x height x length) micropore (sensing channel) to detect the released NPs, (2) a filtering structure consisting an array of 5 μm × 2 μm x 10 μm microchannels to prevent the debris and remaining MPs from blocking the sensing channel, (3) two electrode holes to place a pair of Ag/AgCl electrodes to measure the voltage pulses, and (4) inlet/outlet reservoirs and connection channels. These microfluidic components were fabricated by pouring polydimethylsiloxane (PDMS) onto the SU8 mold, followed by degassing and curing the PDMS for 2 h at 70 °C. Then the inlet/outlet reservoir and electrode holes were punched by 1.5 mm and 1 mm in diameter biopsy punches, respectively. Next, the PDMS slab was treated by air plasma (200 mTorr, 50 W, 50s), followed by being bonded onto a glass substrate to complete the fabrication. The dimensions of the micropore measured by the profilometer (Dektak 150, Veeco Instrument, NY, USA) were 2.28 ± 0.15 μm (width), 2.17 ± 0.22 μm (depth), and 10.87 ± 1.13 μm (length). Finally the Ag/AgCl electrodes (1-mm diameter) were inserted into the electrode holes to complete the RPS.

For each test, the NP suspension was loaded into the inlet reservoir and driven by a syringe pump (KDS Legato 185, KD Scientific) at a flow rate of 36 μL/h. A DC voltage (1 V) was applied across the Ag/AgCl electrodes. The voltage pulse signals by the NPs were amplified with an instrumentation amplifier (AD620BN, Analog Devices Inc, USA) and recorded with an NI – DAQ board (PCI-6133, National Instrument USA) at a sampling rate of 500 kHz. The recorded signals were denoised using a custom MATLAB program to analyze voltage pulses.

2.4. Sample preparation and SNP release

The aptamer-modified SNPs and CS-modified MPs were reacted overnight at either a 10:1 or 100:1 ratio in 100 μL binding buffer solution at room temperature on a rotator. After the reaction, the SNPs-MPs complexes were precipitated by magnetic attraction and the excess/unbound SNPs were collected from the solution. The SNP-MP complexes were washed with DPBS five times or until the measurement of unbound SNPs in DPBS was approximately zero. The intensity of the supernatant containing the excess SNPs from the reaction and the five washes was measured using Nanodrop 3300. For the fluorescent SNPs, the excitation of the material will generate fluorescence emission at a wavelength of 507 nm. The intensity of fluorescence was recorded, and the concentration of SNPs was estimated by a standard curve equation calculated from known SNPs concentrations. The total SNPs attached to MPs was calculated by subtracting the measured excess SNPs in the supernatant from the initial SNPs added to the reaction. The SNPs per MP was estimated by dividing the number of MPs used for the reaction by the

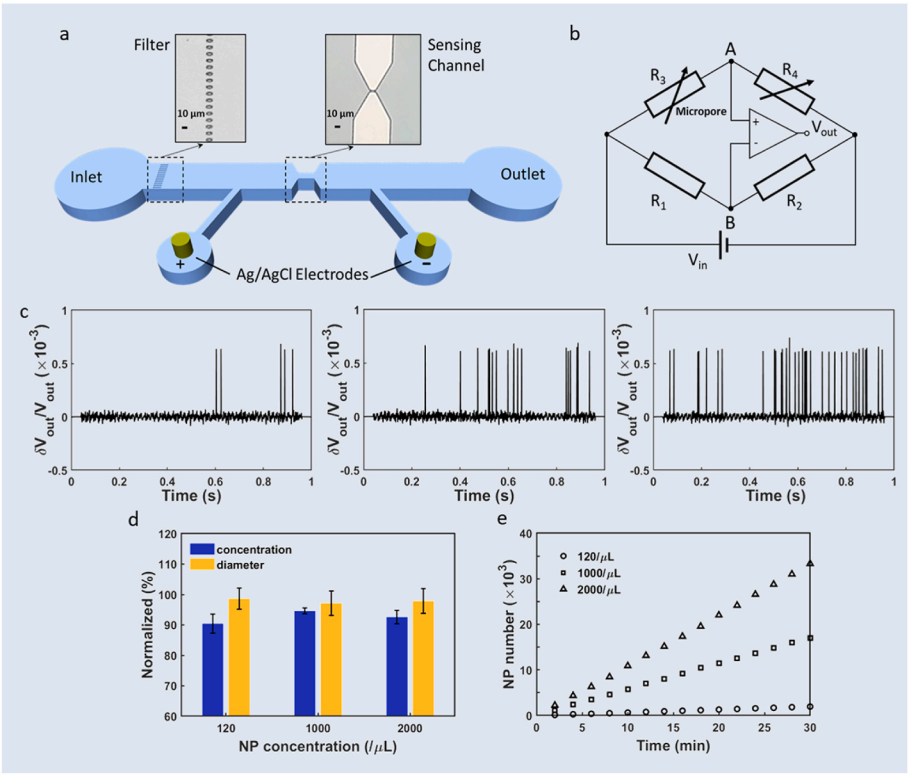

Fig. 2. Microfluidic RPS design and validation. (a) Schematic of microfluidic RPS for NP counting. (b) Diagram of sensing circuit measuring resistive pulses generated by released NPs passing through the micropore. The input voltage Vin was set to 1 V to avoid hydrolysis of DPBS. (c) Voltage pulse plots of known/nominal NP concentrations. Left: 120 NP/μL, Middle: 1000 NP/μL, Right: 2000 NP/μL. (d) Comparison of measured and expected NPs' concentrations and diameters. (e) Kinetic analysis of NP counting.

number of attached SNPs. In addition, flow cytometry was used to examine the shift in the fluorescent intensity of MPs after SNPs attachment.

For concentration-dependent adenosine triggered release studies, 2 × 10^6 MPs were incubated in 50 μL of the release medium at room temperature on a rotator. The release medium was prepared with different adenosine concentration (0.1 nM–10 mM). The adenosine treatment was applied for 1 h. The SNP release medium was collected by separating the MPs via magnetic attraction. For time-dependent release studies, 1 μM and 1 nM adenosine concentrations were chosen for triggering SNP release. The SNP release medium was collected at the predetermined time points (0–60 min). Likewise, the SNP release medium was collected by separating the MPs via magnetic attraction.

3. Results and discussion

3.1. Validation of NP counting

The microfluidic RPS was validated with 500 nm polystyrene NPs (500 ± 50 nm, 95585 - 5 ML – F, Sigma - Aldrich). NPs were taken from the original bottle (with an original concentration of 3.0 × 10^8/μL) and diluted in DPBS. After dilution, NPs at concentrations of 120 NPs/μL, 1000 NPs/μL and 2000 NPs/μL were loaded to the same RPS sensor separately. Each NP sample was measured at a fixed flow rate of 36 μL/h. Resistive pulses (i.e. change of micropore's resistance, ΔR_3) generated by NP passing through the micropore were measured via a Wheatstone bridge (Fig. 2b). Fig. 2c shows typical voltage pulses caused by 500 nm NPs at three concentrations. The relative output voltage change/pulse of the bridge (ΔV_{out})/V_{out}) is:

$$\frac{\Delta V_{out}}{V_{out}} = \left(\frac{R_3 + \Delta R_3}{R_3 + \Delta R_3 + R_4} - \frac{R_1}{R_1 + R_2}\right) \quad (1)$$

Where R_1 and R_2 are the reference resistances (1 k Ohms), R_3 is the base resistance of the micropore, Δ R_3 is the resistance change induced by a NP, R_4 is an adjustable resistor, which was adjusted to be equal to R_3 before each measurement such that the ΔV_{out} is zero when no particle passes the nanopore.

The measured voltage pulses can be converted to resistive pulses ($\Delta R_3/R_3$) by Equation (1). Each resistive pulse represents one NP passing through the micropore. The diameter of each NP can be back calculated from the magnitude of the resistive pulse ($\Delta R_3/R_3$) via Equation (2):

$$\frac{\Delta R_3}{R_3} = \frac{d^3}{LD^2}\left[\frac{D^2}{2L^2} + \frac{1}{\sqrt{1+\left(\frac{D}{L}\right)^2}}\right] F\left(\left(\frac{d}{D}\right)^3\right) \quad (2)$$

$$F(x) = 1 + 1.264x + 1.347x^2 + 0.648x^3 + 4.167x^4 \quad (3)$$

$$D = \sqrt{4A/\pi} \quad (4)$$

where d is the diameter of NP, L and D are the length and characteristic diameter of the rectangular micropore. F is a correction factor related to the ratio of the NP's diameter to micropore diameter and was taken to be 1.008. D is defined in Equation (4), where A is the cross-sectional area of the micropore.

From the recorded voltage pulses, we can calculate the diameters of the NPs by Equations (1) and (2). The NP concentration can be calculated by dividing the count of NPs by the volume of the flow. The measured NP sizes were 490.31 ± 17.26 nm, 485.72 ± 20.13 nm and 489.29 ± 20.35 nm, and the NP concentrations were 108.5 ± 3.7 NPs/μL, 945.9 ± 9.5 NPs/μL, and 1851.8 ± 42.8 NPs/μL. Each standard deviation was obtained from hundreds of NPs of each sample. Both the measured particle concentrations and sizes are in good agreement with the calculated concentrations and the actual sizes (500 ± 50 nm), as shown in Fig. 2d. The stability of the NP concentration measurement was confirmed by measuring the same NP samples at three different days (Fig. S2 in Supplementary Information). The difference in size measurement may be caused by the off-axis effect (Ni et al., 2020), while the difference in concentration measurement is likely due to the uncertainty

in NP dilution. Kinetic analysis of NPs at different concentrations was illustrated in Fig. 2e. The amount of NPs increased with the increasing observation time. This test confirmed the RPS can accurately detect the concentration and size of NPs. Size specification of this RPS sensor was also experimentally confirmed (Fig. S3 in Supplementary Information).

3.2. Characterization of SNP-MP complex

DNAs were first attached to the SNPs and MPs using biotin-streptavidin interactions. The number of DNAs attached per particle was indirectly calculated (see details in section 2.4). Due to the larger surface area of MPs, two orders of magnitude more DNAs were attached to a single MP that to a SNP (Fig. 3a). In addition, the zeta potential of the particles before and after the surface modification was assessed. As shown in Fig. 3b, due to the negative charge of DNA, the zeta potentials of MPs and NPs became more negative after DNA modification. A higher shift in the zeta potential of SNPs was observed. This could be explained by the presence of a larger number of SNPs per w/v % compared to MPs as the same w/v % of MPs and SNPs was used for measurement. Fig. 3a and b confirmed the DNA attachment on the surface of the particles. After the formation of SNP-MP complexes, an inverted fluorescent microscope (Olympus IX73) and scanning electron microscope (SEM, Mag = 15.00 KX) were used to verify the SNPs attachment to the MPs at various SNP:MP ratios, i.e. 0:1 (No NPs), 10:1 and 100:1 as shown in Fig. 3c. A fluorescent signal was detected after the FITC labeled SNPs attached to the CS-MPs. As more SNPs attached per MP, a higher fluorescent intensity per unit area was observed. Similarly, more attached SNPs were observed for 1:100 ratio compared to 1:10. Fig. 3d showed a significant shift in the FITC signal intensity after the SNPs attachment. Moreover, the FITC signal increased approximately 10-fold when the SNP:MP ratio increased from 10:1 to 100:1 ratio, indicating more SNP attachment per MP (Fig. 3d). These flow cytometry results confirmed the observations under the fluorescent microscope. The number of SNPs attached per MP was calculated indirectly from the excess SNPs remaining in the solution after the reaction. As shown in Fig. 3e, the calculated number of attached SNPs per MP was 44.2 ± 8.7 when NP:MP ratio was 100:1 and 7.5 ± 0.5 for 10:1. The subsequent experiments were conducted at NP:MP ratio of 100:1.

3.3. Biomolecule detection

Adenosine was used as the target biomolecule to prove this detection method. Adenosine which forms inside all human cells, plays a dynamic role in regulating cell physiology function and modulating disease processes (Fredholm, 2007; Liu and Xia, 2015; Sheth et al., 2014). Excessive extracellular adenosine contributes to chronic disease progression (Karmouty-Quintana et al., 2013). Therefore, adenosine concentration can be considered as a factor for disease diagnosis and therapy evaluation.

To explore the SNP release process, we measured the released SNP concentration at different incubation times. Two adenosine concentrations, 1 nM and 1 μM, were chosen for time-dependent studies. Release medium was incubated with the SNP-MP complexes for 5 min, 10 min, 20 min, 40 min or 60 min. The released SNPs were collected at each timepoint and counted by the RPS. Each experiment was performed in triplicate. The results are shown in Fig. 4a and b. The concentration of released SNPs increased with increasing incubation time. For each adenosine concentration, the concentration of released SNP increased dramatically from 5 min to 40 min. After 40 min, the SNP release slowed down, especially for the lower adenosine concentration (e.g. 1 nM). The released SNPs ratio (for 1 μM: 1 nM adenosine concentration) peaks at nearly 12:1 during the initial stages of incubation (first 5 min), and stabilizes at approximately 3:1 after 20 min of incubation (Fig. 4c). This study shows that a longer incubation time reduces the variability in SNP release. Hence, we chose the 60 min incubation time to ensure sufficient SNP release. However, a shorter release time can be chosen for a faster detection with reduced sensitivity.

Before mixing adenosine samples with SNP-MP complexes, we first measured the background SNP concentration of the SNP-MP solution due to the presence of residual SNPs in the solution. The residual SNPs were separated from the solution by centrifugation and counted using the RPS. This background concentration was removed in the subsequent

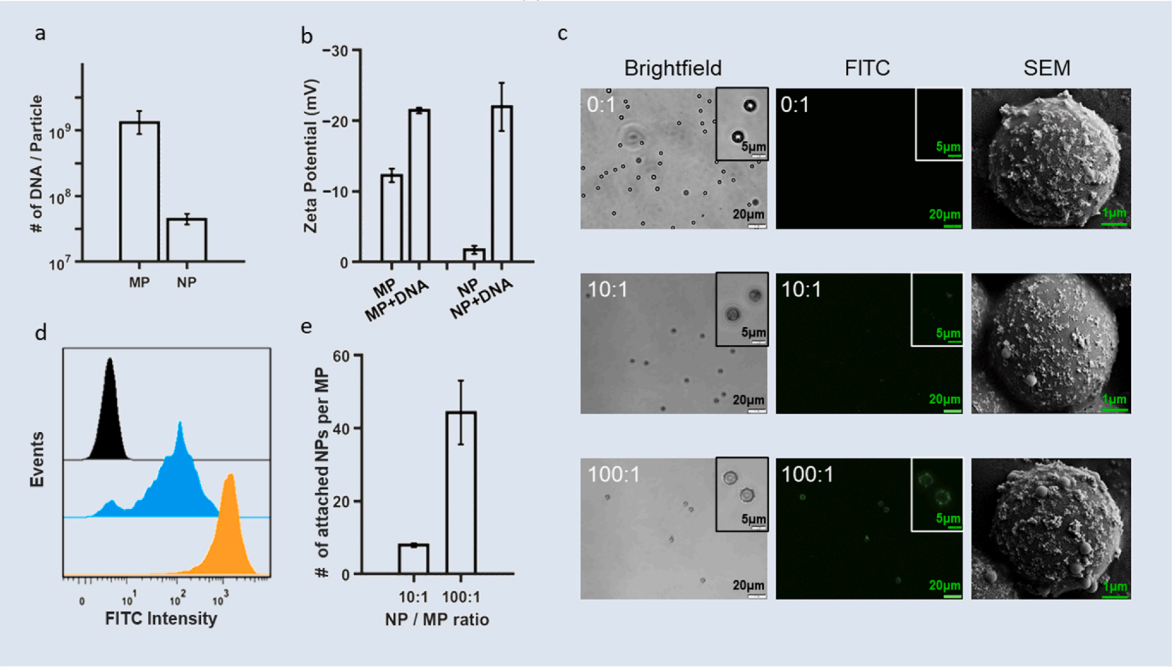

Fig. 3. Formation and characterization of microparticle-nanoparticle (MP-NP) complexes. (a) Number of DNA sequence bound per particle. (b) Zeta potential of unconjugated and DNA conjugated particles. (c–e) Examination of NP to MP ratio in hybridization reaction. (c) Representative images of NP-MP complexes. (d) Flow cytometry analysis of NP-MP complexes. Black: 0:1, Blue: 10:1, Orange: 100:1. (e) Average number of NPs bound to one MP. (For interpretation of the references to color in this figure legend, the reader is referred to the Web version of this article.)

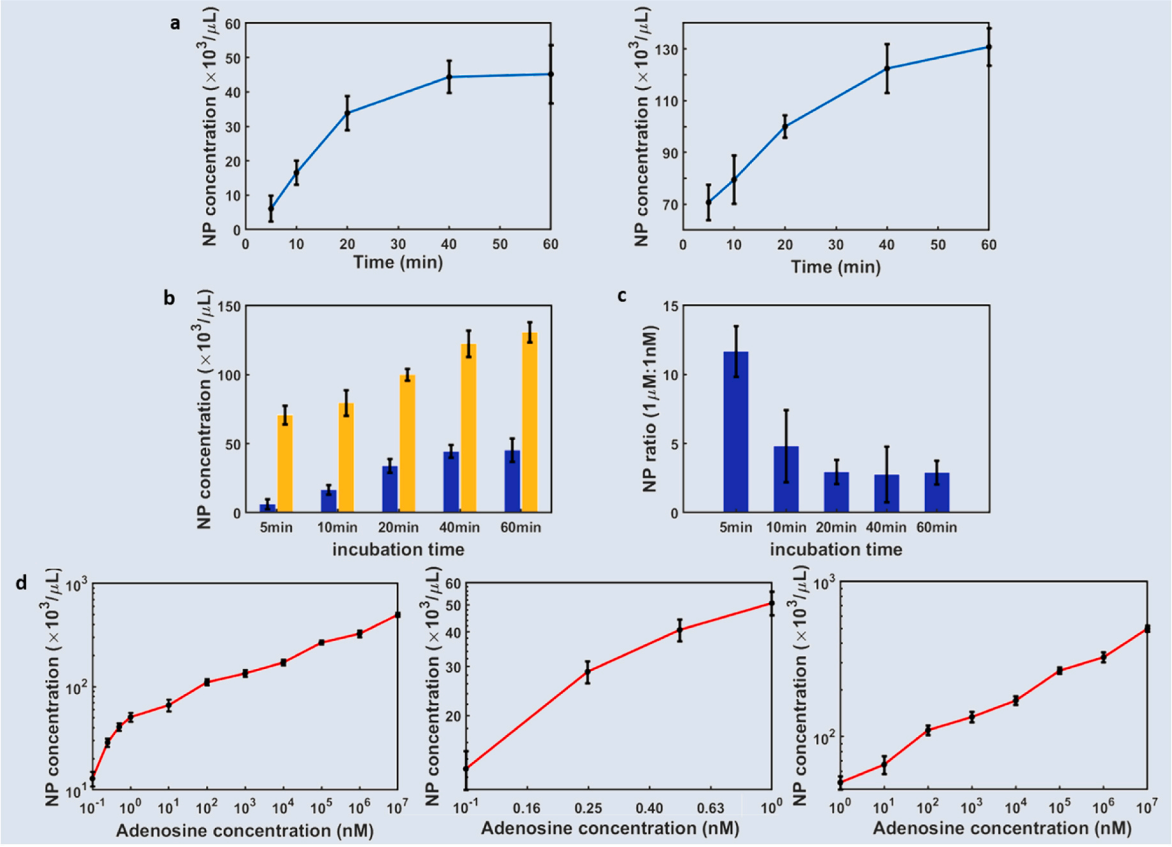

Fig. 4. Experimental results. (a) The released SNP concentration at different incubation time, ranging from 5 min to 60 min. Left: the concentration of adenosine was 1 nM. Right: the concentration of adenosine was 1 μM. Each error bar represents standard deviation of 3 separate measurements from 3 batches. (b) Comparison of NP release over time. Blue: the concentration of adenosine was 1 nM. Orange: the concentration of adenosine was 1 μM. (c) Enhancement efficiency of a higher target molecule concentration with respect to incubation time. Error bars represent the standard deviation calculated from 3 separate measurements of 3 sample replicates. (d) The released SNP concentration measured by the RPS vs adenosine concentration. (For interpretation of the references to color in this figure legend, the reader is referred to the Web version of this article.)

measurements of adenosine samples. Detailed data of blank groups is provided in the Supplementary Information (Section 3). Adenosine samples with concentrations ranging from 0.1 nM to 10 mM were mixed with the SNP-MP complexes. After incubating the SNPs-MPs with adenosine sample for 1 h, the medium was centrifuged to pellet the MPs and collect the supernatant containing the released SNPs. Next, the collected samples were diluted to 300 μL (1:15 dilution) with DPBS to avoid clogging the micropore because of the high concentration of SNPs. Before testing, a vortex mixer was used to agitate the released SNP samples to reduce the aggregation of SNPs. After agitation, the SNP samples were observed under a microscope to ensure the SNPs were uniformly dispersed. The SNPs were then counted by the resistive pulse sensor. Each sample was measured for 1 h at a flow rate of 36 μL/h. The released SNP concentration was calculated from SNP counts.

The relationship between the released SNP concentration and adenosine concentration is shown in Fig. 4d. This result shows the released SNP concentration increased as the adenosine concentration increased. A log scale was used for both the horizontal and vertical axes. At adenosine concentrations from 0.1 nM to 10^1 nM, the released SNP concentration increased faster than at higher concentrations (from 10^1 nM to 10^7 nM). Future research may be conducted to understand this mechanism using both experiments and modeling analysis.

Next we performed a 4 parameter logistic regression (Holstein et al., 2015; Tholen et al., 2004) on the date shown in the middle figure of Fig. 4d:

$$N_{SNP} = d + \frac{a-d}{1+\left(\frac{M}{c}\right)^b} \tag{5}$$

where a, b, c, d could be obtained from the logistic regression, and N_{SNP} is the SNP concentration. M is the adenosine concentration. We then calculated the lower detection limit (LOD) of the SNP measurements following the method by Holstein et al., (2015), which was then plugged in Equation (5) to obtain the LOD of adenosine concentration. Details about the LOD calculations are provided in Section 4 in the Supplementary Information. The LOD of adenosine concentration was calculated to be 0.168 nM (44.85 pg/mL). In comparison to a standard ELISA for Adenosine a1 Receptor ELISA Kit (detection range from 0.313 ng/mL – 20 ng/mL), our method achieved a lower LOD and wider detection range. Compared to other detection methods using aptamer modified NPs (Alsager et al., 2014; Billinge et al., 2014; Billinge and Platt, 2015; Li et al., 2015a; Maugi et al., 2021; Mayne et al., 2018), which typically can measure a biomolecule concentration up to 400 nM (Supplementary Information, Table S2), our method has a larger detection range.

4. Discussion

Our developed method has great promise to make a lab-on-a-chip device to enable ultra-sensitive detection of small biomolecules. Although the aptamer-conjugated SNPs were attached to MPs in this work, they can be attached to micropillar structures fabricated in a microchannel. This will allow the sample loading, SNP release and SNP

counting to be integrated in one chip. Additionally, although only adenosine was tested, in principle, aptamers with high specificity and selectivity can be identified in vitro for any target ranging from small molecules (i.e. metabolites) to large molecules (i.e. proteins), allowing the development of biosensors for multiplexed analysis. To date, aptamers have been used for recognizing a variety of small biomolecules including neurotransmitters (Peaston and Weinkove, 2004; Robinson et al., 2003), amino acids (Gokmen et al., 2012; Omidinia et al., 2014; Tyler, 2000), dietary minerals (Miao et al., 2014; Seki et al., 2010) as well as proteins and whole cells (Hermann and Patel, 2000; Hicke et al., 2001; Zhou and Rossi, 2017). The sensitivity of the detection can be further improved using smaller NPs (e.g. 100 nm NPs), as demonstrated by Billinge et al. (Billinge and Platt, 2015), owing to the ability to attach a larger number of smaller NPs to the MP surface as a result of their smaller binding area and reduced steric hindrance. Thus, even a small amount of analyte could trigger the release of NPs. However, detecting NPs with very small size would require a nanopore, which have to be fabricated using expensive nanofabrication facilities. In addition, nanopore has a low throughput and is easy to be clogged. Therefore, in this study, we chose to use a micropore and a filtering structure instead of a nanopore to avoid the above-mentioned issues.

Worth mentioning here the potentials of utilizing a combination of aptamer modified NPs and RPS to detect biomolecules have also been explored by other research groups. Li et al. developed a high resolution detection method (Li et al., 2015b) based on hybridized aptamer with a ssDNA probe which is modified with a ferrocenecucurbit-[7]uril nano object. Target analytes (i.e. $VEGF_{121}$) caused the aptamer– probe duplex to unbind and release the DNA probe. A α-Hemolysin nanopore based RPS was used to monitor the signature resistive pulse signal by the DNA probe. While the method can achieve high resolution (i.e., pM level), it requires the translocation of ssDNA through the nanopore one by one to generate signature signals; each ssDNA translocation took a long time (e.g. 10s) (Li et al., 2015b). Hence the detection throughput is very low. In addition, any residual aptamer-dsDNA complex may block the pore and disfunction the detection. Recently a method (Billinge and Platt, 2015) utilizing aptamer modified MPs and NPs was demonstrated for detecting thrombin (molecular weight of 36,000 Da), but limited by a narrow detection range (i.e., 1–10 pM). Our developed method presented an effective approach for small biomolecule detection with high sensitivity, high throughput and large dynamic range.

5. Conclusion

We reported a new ultrasensitive biomolecule detection method based on molecular recognition and NP counting. In this method, specific CS-conjugated MPs and aptamer-modified SNPs are used as sensing materials. A microfluidic RPS was used to detect the released SNPs triggered by targeted biomolecules. Adenosine was used as a model small biomolecule. The released SNPs increased as the biomolecule concentration increased. Compared to current other biomolecule detection methods, our method enables higher sensitivity and a larger detection range. In addition, it requires minimum sample preparation and eliminates the need for tedious calibration. This method shows great potential for small biomolecule detection at ultra low concentration and will be applicable in vast array of biological applications.

Author Contributions

Ruiting Xu, Lidya Abune, Brandon Davis and Jiang Zhe drafted the manuscript. Ruiting Xu and Leixin Ouyang contributed the fabrication of micropore and experiments. Lidya Abune and Brandon Davis contributed to the design and synthesis of SNP-MP release system. Yong Wang and Ge Zhang reviewed and edited the manuscript. Jiang Zhe directed the project.

$: R.X. and L.A. contributed equally.

Declaration of competing interest

The authors declare that they have no known competing financial interests or personal relationships that could have appeared to influence the work reported in this paper.

Acknowledgements

This work was supported by the National Science Foundation of USA under award numbers DBI 1911526, ECCS 1905786 and CBET 1802953.

Appendix A. Supplementary data

Supplementary data to this article can be found online at https://doi.org/10.1016/j.bios.2022.114023.

References

Alsager, O.A., Kumar, S., Willmott, G.R., McNatty, K.P., Hodgkiss, J.M., 2014. Biosens. Bioelectron. 57, 262–268.
Arima, A., Tsutsui, M., Harlisa, I.H., Yoshida, T., Tanaka, M., Yokota, K., Tonomura, W., Taniguchi, M., Okochi, M., Washio, T., Kawai, T., 2018. Sci. Rep. 8, 16305.
Billinge, E.R., Broom, M., Platt, M., 2014. Anal. Chem. 86, 1030–1037.
Billinge, E.R., Platt, M., 2015. Anal. Methods 7, 8534–8538.
Byrne, B., Stack, E., Gilmartin, N., O'Kennedy, R., 2009. Sensors 9, 4407–4445.
Chang, C.C., Chen, C.P., Wu, T.H., Yang, C.H., Lin, C.W., Chen, C.Y., 2019. Nanomaterials 9.
Chen, Y.J., Chen, M., Hsieh, Y.C., Su, Y.C., Wang, C.H., Cheng, C.M., Kao, A.P., Wang, K. H., Cheng, J.J., Chuang, K.H., 2018. Sci. Rep. 8, 17868.
DeBlois, R.W., Bean, C.P., 1970. Review of. Sci. Instrum. 41, 909–916.
Fredholm, B.B., 2007. Cell Death Differ. 14, 1315–1323.
Fu, W., Alam, T.M., Li, J., Bustamante, J., Lien, T., Adams, R.W., Teat, S.J., Stokes, B.J., Yang, W., Liu, Y., Lu, J.Q., 2020. J. Am. Chem. Soc. 142, 16651–16660.
Garibyan, L., Avashia, N., 2013. J. Invest. Dermatol. 133, 1–4.
Gokmen, V., Serpen, A., Mogol, B.A., 2012. Anal. Bioanal. Chem. 403, 2915–2922.
Green, S.J., Venkatramanan, R., Naqib, A., 2015. PLoS One 10, e0128122.
Hahm, B.K., Bhunia, A.K., 2006. J. Appl. Microbiol. 100, 1017–1027.
Han, Y., Wu, H., Liu, F., Cheng, G., Zhe, J., 2014. Anal. Chem. 86, 9717–9722.
Han, Y., Wu, H., Liu, F., Cheng, G., Zhe, J., 2016. Biomicrofluidics 10, 024109.
Harrell, C.C., Choi, Y., Horne, L.P., Baker, L.A., Siwy, Z.S., Martin, C.R., 2006. Langmuir 22, 10837–10843.
Hearty, S., Leonard, P., Quinn, J., O'Kennedy, R., 2006. J. Microbiol. Methods 66, 294–312.
Heaton, I., Platt, M., 2019. Anal. Chem. 91, 11291–11296.
Hermann, T., Patel, D.J., 2000. Science 287, 820–825.
Hetzke, T., Vogel, M., Gophane, D.B., Weigand, J.E., Suess, B., Sigurdsson, S.T., Prisner, T.F., 2019. RNA 25, 158–167.
Hianik, T., Ostatna, V., Sonlajtnerova, M., Grman, I., 2007. Bioelectrochemistry 70, 127–133.
Hicke, B.J., Marion, C., Chang, Y.F., Gould, T., Lynott, C.K., Parma, D., Schmidt, P.G., Warren, S., 2001. J. Biol. Chem. 276, 48644–48654.
Holstein, C.A., Griffin, M., Hong, J., Sampson, P.D., 2015. Anal. Chem. 87, 9795–9801.
Huizenga, D.E., Szostak, J.W., 1995. Biochemistry 34, 656–665.
Kalra, P., Dhiman, A., Cho, W.C., Bruno, J.G., Sharma, T.K., 2018. Front Mol Biosci 5, 41.
Karmouty-Quintana, H., Xia, Y., Blackburn, M.R., 2013. J. Mol. Med. (Berl.) 91, 173–181.
Lai, J., Li, S., Shi, X., Coyne, J., Zhao, N., Dong, F., Mao, Y., Wang, Y., 2017. Chem. Sci. 8, 7306–7311.
Li, T., Liu, L., Li, Y., Xie, J., Wu, H.-C., 2015a. Angew. Chem. 127, 7678–7681.
Li, T., Liu, L., Li, Y., Xie, J., Wu, H.C., 2015b. Angew Chem. Int. Ed. Engl. 54, 7568–7571.
Lin, C.H., Patei, D.J., 1997. Chem. Biol. 4, 817–832.
Liu, F., Kc, P., Ni, L., Zhang, G., Zhe, J., 2018a. Organogenesis 14, 67–81.
Liu, G., Lu, M., Huang, X., Li, T., Xu, D., 2018b. Sensors 18.
Liu, H., Lei, Y., 2021. Biosens. Bioelectron. 177, 112901.
Liu, H., Xia, Y., 2015. J. Appl. Physiol. 119, 1173–1182, 1985.
Liu, J., Lu, Y., 2005. Angew Chem. Int. Ed. Engl. 45, 90–94.
Liu, J., Lu, Y., 2006a. Nat. Protoc. 1, 246–252.
Liu, J., Lu, Y., 2006b. Adv. Mater. 18, 1667–1671.
Maugi, R., Gamble, B., Bunka, D., Platt, M., 2021. Talanta 225, 122068.
Maugi, R., Salkenova, Z., Platt, M., 2020. Med. Dev.Sensor. 3.
Mayne, L., Lin, C.Y., Christie, S.D.R., Siwy, Z.S., Platt, M., 2018. ACS Nano 12, 4844–4852.
Maysinger, D., Ji, J., Hutter, E., Cooper, E., 2015. Front. Neurosci. 9, 480.
Miao, P., Tang, Y., Wang, B., Han, K., Chen, X., Sun, H., 2014. Analyst 139, 5695–5699.
Ni, L., Shaik, R., Xu, R., Zhang, G., Zhe, J., 2020. ACS Sens. 5, 527–534.
Ni, S., Zhuo, Z., Pan, Y., Yu, Y., Li, F., Liu, J., Wang, L., Wu, X., Li, D., Wan, Y., Zhang, L., Yang, Z., Zhang, B.T., Lu, A., Zhang, G., 2021. ACS Appl. Mater. Interfaces 13, 9500–9519.
Omidinia, E., Shadjou, N., Hasanzadeh, M., 2014. Appl. Biochem. Biotechnol. 172, 2070–2080.
Peaston, R.T., Weinkove, C., 2004. Ann. Clin. Biochem. 41, 17–38.

Peng, R., Li, D., 2018. Talanta 184, 418–428.
Powledge, T.M., 2004. Adv. Physiol. Educ. 28, 44–50.
Prante, M., Segal, E., Scheper, T., Bahnemann, J., Walter, J., 2020. Biosensors 10.
Robinson, D.L., Venton, B.J., Heien, M.L., Wightman, R.M., 2003. Clin. Chem. 49, 1763–1773.
Ruscito, A., DeRosa, M.C., 2016. Front. Chem. 4, 14.
Sakamoto, S., Putalun, W., Vimolmangkang, S., Phoolcharoen, W., Shoyama, Y., Tanaka, H., Morimoto, S., 2018. J. Nat. Med. 72, 32–42.
Seki, T., Yamamoto, M., Kimura, H., Tsuiki, M., Ono, M., Miki, N., Takano, K., Sato, K., 2010. Endocr. J. 57, 735–744.
Sexton, L.T., Horne, L.P., Sherrill, S.A., Bishop, G.W., Baker, L.A., Martin, C.R., 2007. J. Am. Chem. Soc. 129, 13144–13152.
Sha, J., Hasan, T., Milana, S., Bertulli, C., Bell, N.A., Privitera, G., Ni, Z., Chen, Y., Bonaccorso, F., Ferrari, A.C., Keyser, U.F., Huang, Y.Y., 2013. ACS Nano 7, 8857–8869.
Sheth, S., Brito, R., Mukherjea, D., Rybak, L.P., Ramkumar, V., 2014. Int. J. Mol. Sci. 15, 2024–2052.
Song, S., Wang, L., Li, J., Fan, C., Zhao, J., 2008. Trac. Trends Anal. Chem. 27, 108–117.
Song, Y., Zhang, J., Li, D., 2017. Micromachines 8.
Tang, H., Wang, H., Yang, C., Zhao, D., Qian, Y., Li, Y., 2020. Anal. Chem. 92, 3042–3049.
Tholen, D.W., Linnet, K., Kondratovich, M.V., Armbruster, D.A., Garrett, P.E., Jones, R.L., Kroll, M.H., Lequin, R.M., Pankratz, T., Scassellati, G.A., Schimmel, H.G., Tsai, J., 2004. NCCLS. Wayne PA.
Tyler, M.I., 2000. Methods Mol. Biol. 159, 1–7.
Wang, L., Liu, X., Hu, X., Song, S., Fan, C., 2006. Chem. Commun. 3780–3782.
Wang, X., Cohen, L., Wang, J., Walt, D.R., 2018. J. Am. Chem. Soc. 140, 18132–18139.
Wright, P.F., Nilsson, E., Van Rooij, E.M., Lelenta, M., Jeggo, M.H., 1993. Rev Sci Tech 12, 435–450.
Yang, L., Yamamoto, T., 2016. Front. Microbiol. 7, 1500.
Zhou, J., Rossi, J., 2017. Nat. Rev. Drug Discov. 16, 181–202.
Zhou, K., Li, L., Tan, Z., Zlotnick, A., Jacobson, S.C., 2011. J. Am. Chem. Soc. 133, 1618–1621.